

## Supporting Information

### Nickel-Oxide embedded Laser-Induced Graphene for High-Performance Supercapacitors

Hani Porat<sup>a</sup>, Aneena Lal<sup>a</sup>, Asmita Dutta<sup>a</sup>, Manish Kumar Yadav<sup>a</sup>, Divya Catherin Sesu<sup>a</sup>,  
Refael Minnes<sup>b</sup>, Arie Borenstein<sup>a,\*</sup>.

a- Department of Chemical Sciences, Ariel University, Ariel, Israel

b- Department of Physics, Ariel University, Ariel, Israel

\*- Corresponding author, email: arieb@ariel.ac.il

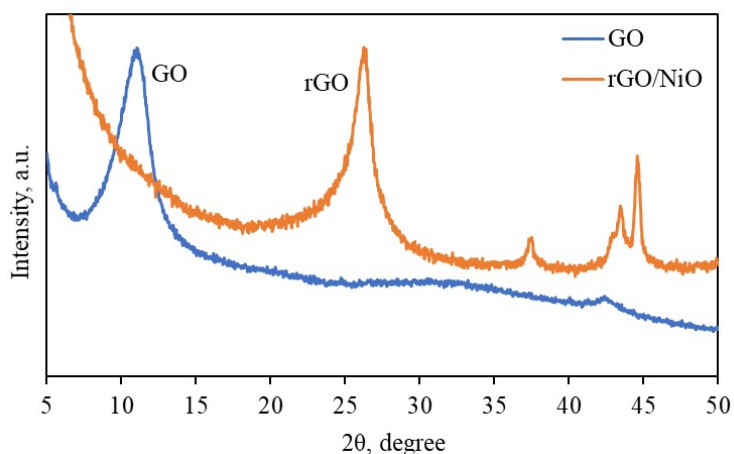


Figure S1. XRD patterns of GO and rGO-Ni-5.

The rGO/NiO nanocomposite's recorded XPS profile is displayed in Figure S2. The survey spectrum shows that the composite is composed of carbon, nickel, and oxygen components. In order to determine surface oxidation, the major peaks of C 1s, O 1s, and Ni 2p were deconvoluted into many signals at higher resolution spectra. Sulfur and nitrogen impurities remain from the GO synthesis process, as seen in the graph and Table S1. We estimate that the contaminants do not interfere with the following processes since, as Table S1 shows, their fraction by weight is low.

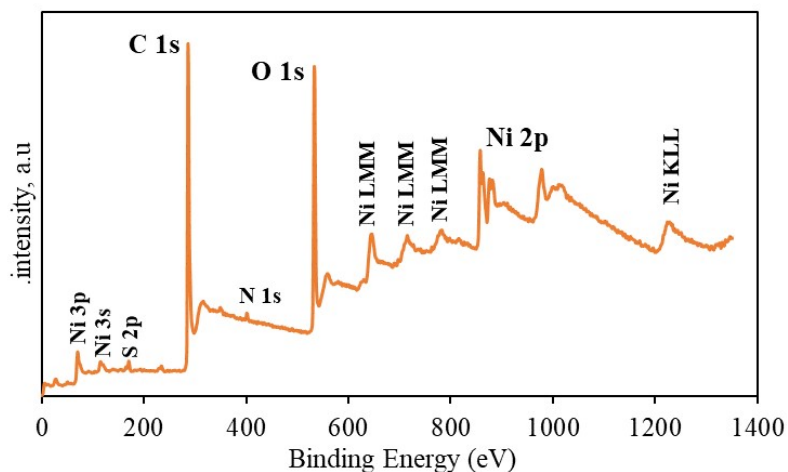


Figure S2. XPS spectra of rGO-Ni-5 nanocomposites survey scan.

Table S1: Atomic surface concentration (at.%) determined by XPS quantitative analysis of rGO-Ni-5 nanocomposites.

Name	Peak BE	FWHM eV	Atomic %
S2p	169	2.37	1.33
N1s	400.26	2.1	1.08
C1s Scan A	284.99	1.26	42.64
C1s Scan B	286.44	1.63	14.43
C1s Scan C	288.65	2.01	8.83
C1s Scan D	291.19	2	1.61
O1s Scan A	531.98	1.84	17.39
O1s Scan B	533.72	2	6.97
O1s Scan C	530.27	0.95	0.88
Ni2p	856.67	3.43	4.84

Based on Atomic surface concentration (at.%) determined by XPS, the C/O ratio before and after the laser irradiation is calculated. Anticipatedly, laser irradiation lowers the oxygen content from 36% to 24 %, increasing the carbon to oxygen ratio from 1.6 to 2.8.

Table S2: Atomic surface concentration (at.%) determined by XPS quantitative analysis of GO and rGO.

	C	O	C/O ratio
GO	60	36	1.6
rGO	67	24	2.8

CHNS analysis was also performed on the samples to ascertain the proportion of carbon to oxygen and the quantity (wt.%) of each element in them both before and after laser treatment. The oxygen level dropped from 57% to 26%, and the carbon/oxygen ratio increased from 0.4 to 0.85, as predicted, proving that GO was successfully converted into rGO.

Table S3: CHNS properties (wt.%) of GO and rGO.

	C	H	O	N	S	C/O ratio
GO	23.98	4.28	57.58	3.40	0.39	0.42
rGO	22.42	3.31	26.52	0.99	.0.00	0.85

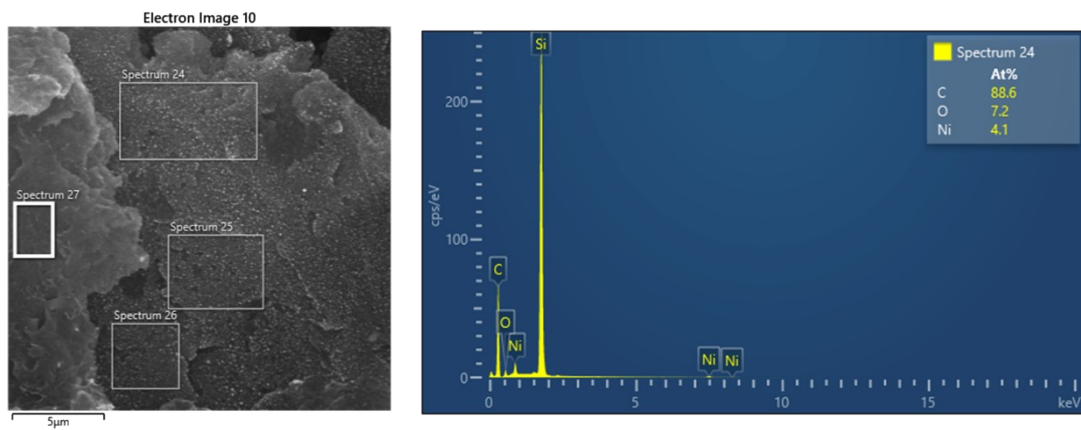
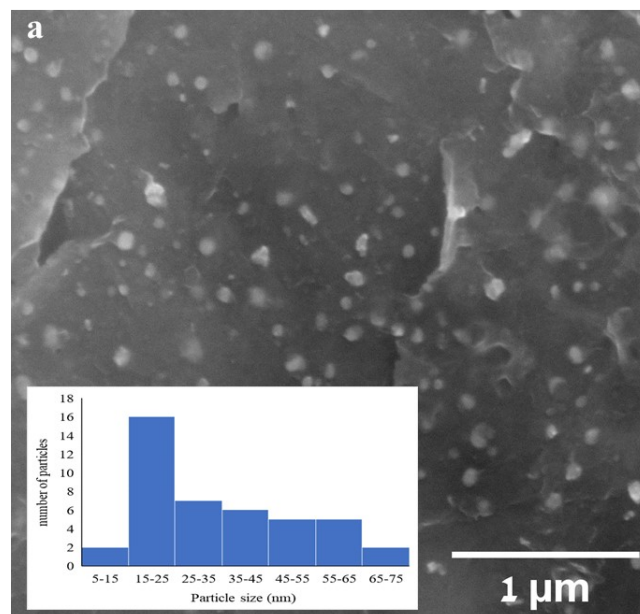


Figure S3. EDX spectra of rGO-Ni-3.



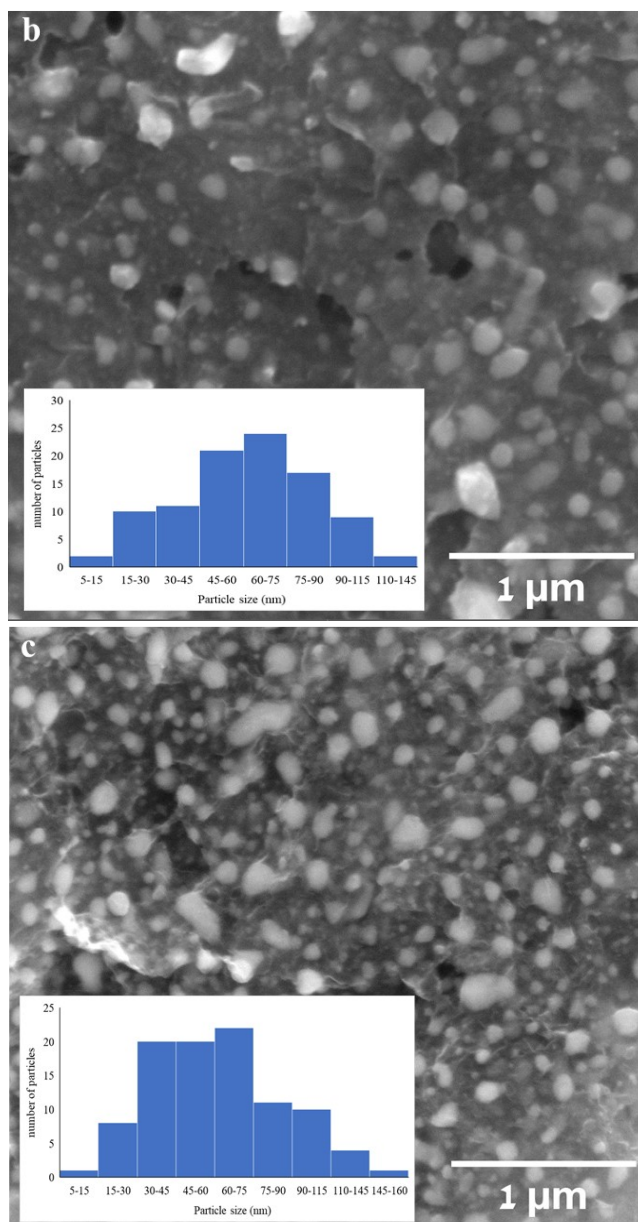
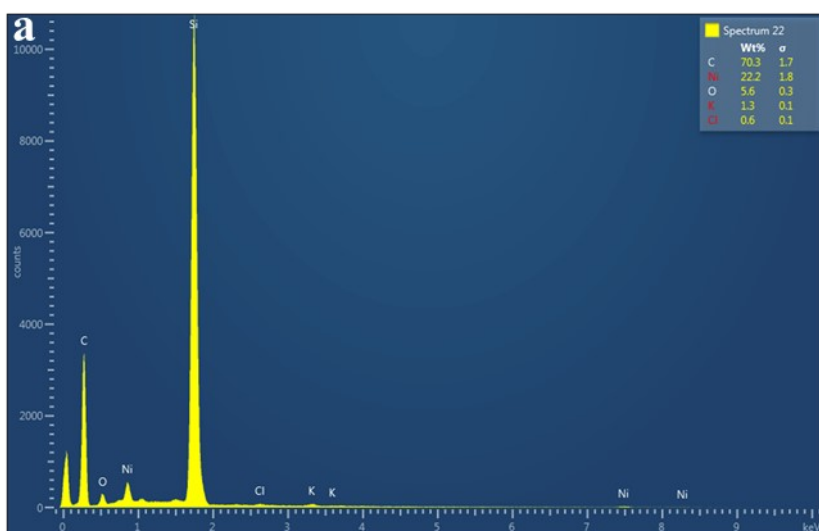


Figure S4. image captured by high resolution scanning electron microscopy of prepared a. rGO-Ni-2 b. rGO-Ni-5 c. rGO-Ni-6 which was synthesized chemically. *Inset.* histogram of the nickel particles size.



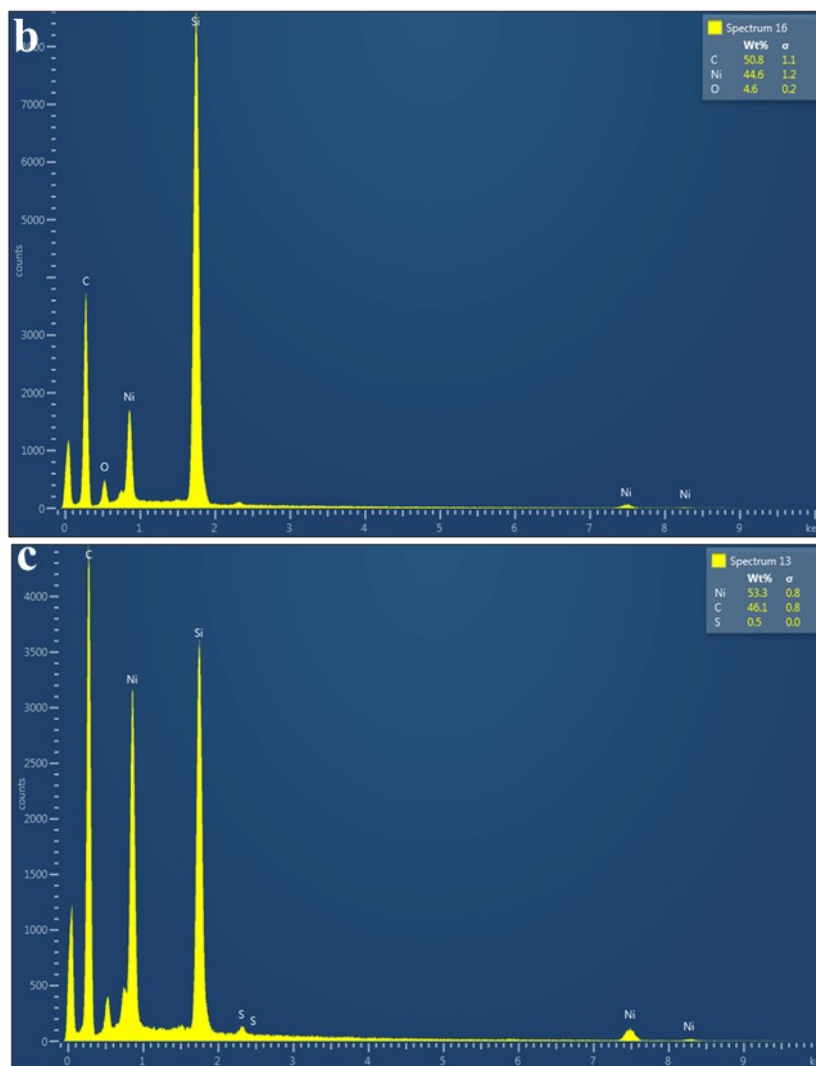


Figure S5. EDX spectra of a. rGO-Ni-2. b. rGO-Ni-5. c. rGO-Ni-6.

The specific surface areas and material porosity are estimated using the  $N_2$  adsorption-desorption experiment conducted at 77 K. The absorption-desorption curves imply developed mesoporosity.<sup>1</sup> According to the IUPAC classification, the rGO-Ni isotherm (Figure S6a) indicates a type IV mesoporous structure with H3 hysteresis loops. The rGO-Ni composite's BET surface area is  $99.2392 \pm 0.3910 \text{ m}^2/\text{g}$  and pore volume is  $0.29 \text{ cm}^3/\text{g}$ . Interestingly, while the surface area of only rGO treated by laser is  $356 \text{ m}^2/\text{g}$ , according to Kwon et al.<sup>2</sup> Expectedly, the addition of nickel oxide particles reduced the surface area of rGO-Ni.

Pore size distribution (Figure S6b) indicates combined micro- and microporosity. The large volume of mesopores ranges from 2 to 20 nm, with an average pore size of 9.3 nm, which can facilitate fast ion diffusion. Micropores range, which is referenced in the inset, falls into the

range of less than 1 nm, with a total area of  $101.57 \pm 1.37 \text{ m}^2/\text{g}$ , contribute to the surface area, which is crucial for EDLC.<sup>3</sup>

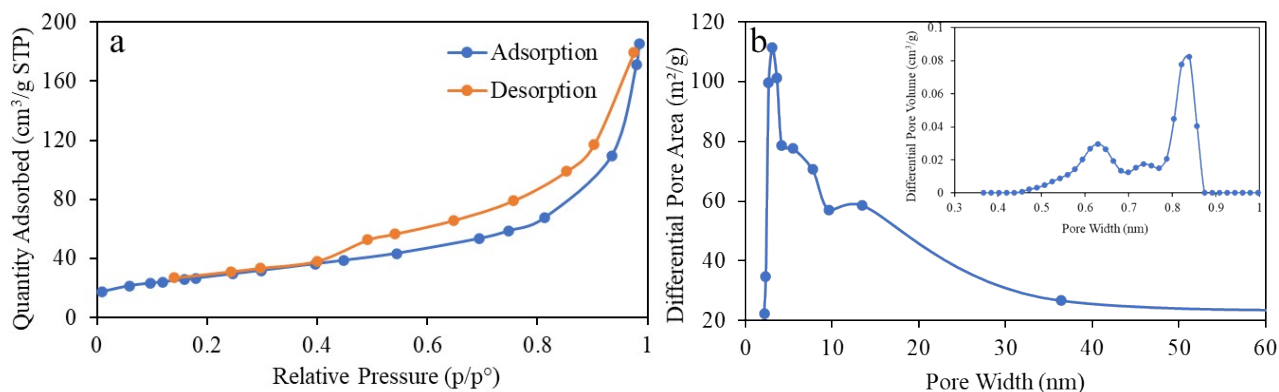


Figure S6. BET surface area analysis of rGO-Ni-6 composites: (a)  $\text{N}_2$  adsorption–desorption isotherm. (b) porosity distribution of the rGO-Ni-6nanocomposite (micropore distribution in the inset).

Figure S7. Charge/discharge curves at a constant current density of 1 A/g for the rGO-Ni-3 electrode with 6 M KOH and 0.5 M  $\text{Na}_2\text{SO}_4$  aqueous electrolyte solutions.

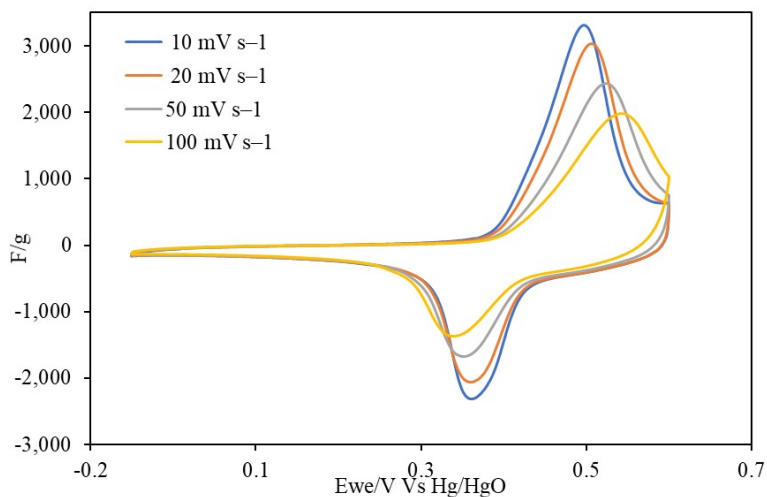


Figure S8. CV curves of the rGO/NiO composites at different scan rates. The electrolyte is 6 M KOH solution.

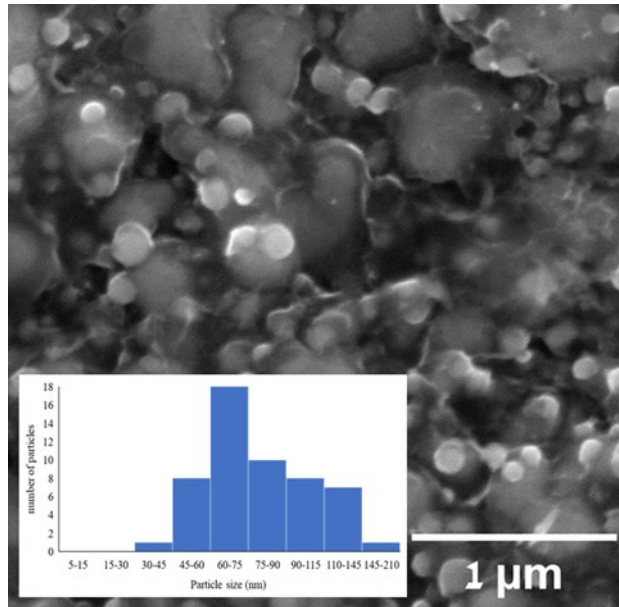


Figure S9. image captured by high resolution scanning electron microscopy of prepared rGO-Ni-6 which was synthesized chemically after cycling. *Inset.* histogram of the nickel particles size

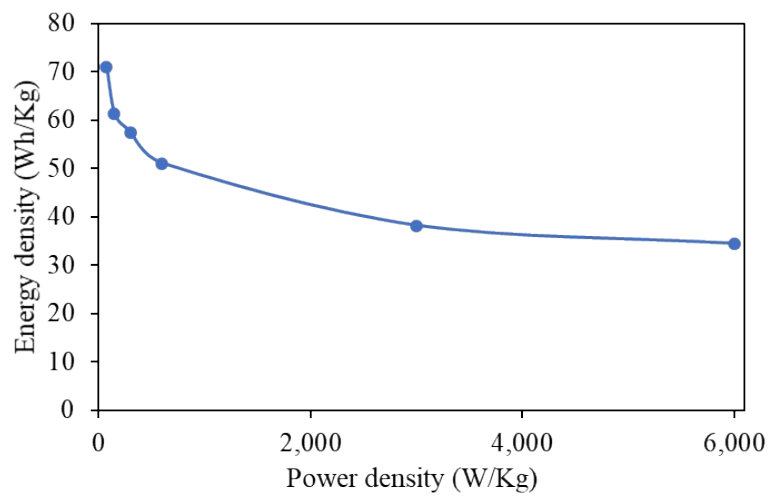


Figure S10. Regone plot for rGO-Ni-6.

## References

- 1 M. Thommes and K. A. Cychosz, *Adsorption*, 2014, 20, 233–250.
- 2 S. Kwon, Y. Yoon, J. Ahn, H. Lim, G. Kim, J. H. Kim, K. B. Choi and J. J. Lee, *Carbon N Y*, 2018, 137, 136–145.
- 3 S. Thomas, A. B. Gueye and R. K. Gupta, Eds., *Nanostructured Materials for Supercapacitors*, Springer International Publishing, Cham, 2022.